Contents lists available at ScienceDirect

Marine Chemistry

journal homepage: www.elsevier.com/locate/marchem

Isotopic constraints on the Si-biogeochemical cycle of the Antarctic Zone in the Kerguelen area (KEOPS)

François Fripiat [a,b,*], Anne-Julie Cavagna [c], Nicolas Savoye [c,d], Frank Dehairs [c], Luc André [a], Damien Cardinal [a,e]

[a] Geology and Mineralogy, Section of Mineralogy and Petrography, Royal Museum for Central Africa, Tervuren, Belgium
[b] Department of Earth and Environmental Sciences, Université Libre de Bruxelles, CP160/02, Av F.D. Roosevelt 50, B1050, Bruxelles, Belgium
[c] Analytical and Environmental Chemistry & Earth System Sciences, Vrije Universiteit Brussel, Brussels, Belgium
[d] Observatoire Aquitain des Sciences de l'Univers, UMR CNRS 6805 EPOC, Laboratoire d'Océanographie Biologique, Arcachon, France
[e] LOCEAN, Université Pierre et Marie Curie, Paris, France

ABSTRACT

Estimation of the silicon (Si) mass balance in the ocean from direct measurements (Si uptake-dissolution rates …) is plagued by the strong temporal and spatial variability of the surface ocean as well as methodological artifacts. Tracers with different sensitivities toward physical and biological processes would be of great complementary use. Silicon isotopic composition is a promising proxy to improve constraints on the Si-biogeochemical cycle, since it integrates over longer timescales in comparison with direct measurements and since the isotopic balance allows to resolve the processes involved, i.e. uptake, dissolution, mixing. Si-isotopic signatures of seawater $Si(OH)_4$ and biogenic silica ($bSiO_2$) were investigated in late summer 2005 during the KEOPS experiment, focusing on two contrasting biogeochemical areas in the Antarctic Zone: a natural iron-fertilized area above the Kerguelen Plateau (<500 m water depth) and the High Nutrient Low Chlorophyll area (HNLC) east of the plateau (>1000 m water depth). For the HNLC area the Si-isotopic constraint identified Upper Circumpolar Deep Water as being the ultimate Si-source. The latter supplies summer mixed layer with 4.0 ± 0.7 mol Si m^{-2} yr^{-1}. This supply must be equivalent to the net annual $bSiO_2$ production and exceeds the seasonal depletion as estimated from a simple mixed layer mass balance (2.5 ± 0.2 mol Si m^{-2} yr^{-1}). This discrepancy reveals that some 1.5 ± 0.7 mol Si m^{-2} yr^{-1} must be supplied to the mixed layer during the stratification period. For the fertilized plateau bloom area, a low apparent mixed layer isotopic fractionation value ($\Delta^{30}Si$) probably reflects (1) a significant impact of $bSiO_2$ dissolution, enriching the $bSiO_2$ pool in heavy isotope; and/or (2) a high Si uptake over supply ratio in mixed layer at the beginning of the bloom, following an initial closed system operating mode, which, however, becomes supplied toward the end of the bloom (low Si uptake over supply ratio) with isotopically light $Si(OH)_4$ from below when the surface $Si(OH)_4$ pool is significantly depleted. We estimated a net integrated $bSiO_2$ production of 10.5 ± 1.4 mol Si m^{-2} yr^{-1} in the AASW above the plateau, which includes a significant contribution of $bSiO_2$ production below the euphotic layer. However, advection which could be significant for this area has not been taken into account in the latter estimation based on a 1D approach of the plateau system. Finally, combining the KEOPS Si-isotopic data with those from previous studies, we refined the average Si-isotopic fractionation factor to -1.2 ± 0.2‰ for the Antarctic Circumpolar Current.

© 2010 Elsevier B.V. All rights reserved.

1. Introduction

The Southern Ocean plays a major role in global circulation and redistributes nutrients toward the surface layer at the global scale via the upper limb of the meridional circulation (Sarmiento et al., 2004, 2007). As a result biogeochemical processes in Southern Ocean surface water have a significant impact on nutrient availability in low latitude surface waters (Sarmiento et al., 2004). In the Southern Ocean, diatoms play a key role in the carbon biological pump, exporting both biogenic silica ($bSiO_2$) and organic carbon to the deep ocean (Buesseler, 1998; Buesseler et al., 2001). The Southern Ocean is the largest High Nutrient Low Chlorophyll (HNLC) area and macronutrient (i.e., nitrate and phosphate) concentrations remain high throughout the year across much of the Antarctic Circumpolar Current (ACC). Dissolved silicon, which is mainly present in the form of silicic acid ($Si(OH)_4$; sometimes referred to as silicate), behaves differently from other macro-nutrients. Unlike for nitrate which remains relatively constant, the region of the ACC between the Antarctic Polar Front (APF) and the Seasonal Ice Zone is marked by an extremely strong $Si(OH)_4$ positive concentration gradient southward (Brzezinski et al., 2001; Quéguiner and Brzezinski, 2002). Diatom biomass and silica prodcution are likely Si-limited during the entire

* Corresponding author. Mailing address: Leuvensesteenweg, 13, B-3080 Tervuren, Belgium. Tel.: +32 27695460; fax: +32 27695432.
E-mail address: ffripiat@ulb.ac.be (F. Fripiat).

productive seasons north of the APF, productive season, while those south of the front become Si-limited only at the end of the growth season (Nelson et al., 2001). The Si–N decoupling and the HNLC characteristic features have been attributed to iron, light and Si co-limitations (Brzezinski et al., 2005; De Baar et al., 2005; Boyd, 2007), along with the processes involved in the so called "silicate pump" the deeper remineralization of Si relative to C and N (Dugdale et al., 1995).

The KErguelen Ocean and Plateau compared Study (KEOPS) was conducted to investigate a naturally iron-fertilized area located to the south-east of the Kerguelen Islands in the Indian sector of the Southern Ocean where a well-developed bloom is observed annually (Mongin et al., 2008; Fig. 1). Results from KEOPS have provided evidence that deep iron-rich waters supply iron to the surface waters over the Kerguelen Plateau through enhanced vertical mixing triggered by internal wave activity (Blain et al., 2007; Park et al., 2008b).

Considering that diatoms are the main contributors to Southern Ocean primary production (Nelson et al., 2002), a better understanding of the Si-biogeochemical cycle is necessary to assess the Southern Ocean biological pump and the fertility potential of the waters exported out of the ACC toward lower latitudes. The interpretation of integrated $bSiO_2$ production–dissolution rates and $bSiO_2$ export is plagued by their strong temporal and spatial variabilities, as well as by artifacts associated with their measurement (e.g., bottle effects,

snapshots and/or sediment trap biases). The isotopic composition of silicon ($\delta^{30}Si$) is a promising proxy to alleviate effects of such temporal and spatial variabilities. $\delta^{30}Si$ signature is also able to trace back sources and the magnitude of transformation of Si. $Si(OH)_4$ uptake by diatoms leaves a clear imprint on the isotopic compositions of both Si $(OH)_4$ and $bSiO_2$. Field studies (Varela et al., 2004; Alleman et al., 2005; Cardinal et al., 2005, 2007; Reynolds et al., 2006; Fripiat et al., 2007; Beucher et al., 2008; Cavagna et al., in press) and controlled laboratory studies (De La Rocha et al., 1997; Milligan et al., 2004) have revealed isotopic fractionation associated with preferential incorporation of ^{28}Si by diatoms. The $^{30}\varepsilon$ fractionation factor ($-1.1 \pm 0.4‰$) reported by De La Rocha et al. (1997) seems to be independent of temperature, species (De La Rocha et al., 1997) and cell size (Cardinal et al., 2007). Recently Demarest et al. (2009) reported an isotopic fractionation associated with $bSiO_2$ dissolution whereby preferentially light Si-isotopes are released ($^{30}\varepsilon = -0.55‰$). By increasing the euphotic $bSiO_2$ dissolution/production ratio the overall isotopic fractionation associated with Si uptake would be dampened.

In this study, we compare Si-isotopic compositions from different water masses above the Kerguelen Plateau (the fertilized area) and off plateau (the HNLC area). We used these signatures to trace the routes of the $Si(OH)_4$ supply to the euphotic layer and to make an attempt to close the Si-biogeochemical budget in this area.
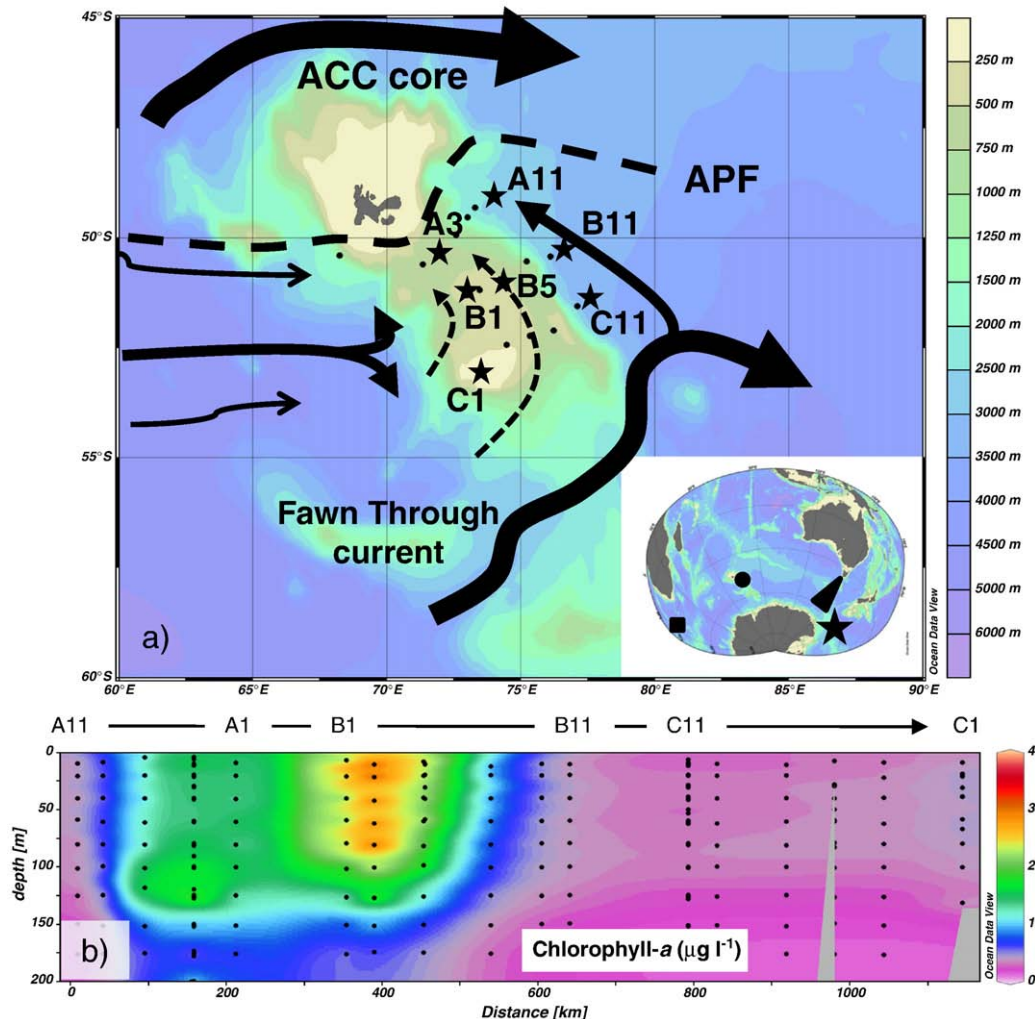
Fig. 1. (a) Map of the study area with bathymetry and geostrophic circulation (black arrows; following Park et al. (2008a) and Zhang et al. (2008)). The Fawn Through splits the Kerguelen Plateaus, and constitutes a favored zonal passage for the circumpolar flow crossing the plateau, "Fawn Through Current" (Park et al., 2008a). The KEOPS stations are represented by black dots, while stars refer to the stations with Si-isotopic signatures available in this study. The hemispheric projection indicates the different Si-isotopic studies in the Southern Ocean: star: Varela et al. (2004); triangle: Cardinal et al. (2005, 2007); star: Cavagna et al. (in press), and dot: KEOPS (this study). ACC: Antarctic Circumpolar Current; APF: Antarctic Polar Front. (b) Chlorophyll-*a* section (0–200 m depth) across the investigated KEOPS stations (data from Uitz et al. (2009)).

2. Material and methods

2.1. The Kerguelen Ocean and Plateau compared Study (KEOPS)

The KEOPS cruise was conducted around the Kerguelen Islands from January 19th to February 13th, 2005, aboard R.V. Marion Dufresne. Its major aim was to investigate the biological pump under natural iron fertilization conditions sustained by the plateau (Blain et al., 2007). The cruise track consisted of three transects (A, B and C; Fig. 1a) across the plateau (bathymetry <500 m) reaching to the off-plateau HNLC area (bathymetry >1000 m). Two reference stations, A3 and C11, were selected as representative for the plateau area and the off-plateau HNLC area, respectively. These reference stations were visited several times. Satellite-derived chlorophyll data for the 2004–2005 season indicated that the bloom started early November, reached its maximum in December and collapsed in February. KEOPS was therefore conducted during the demise of the bloom (Mongin et al., 2008).

2.2. Sampling and analyses

Seawater was collected using CTD Rosette mounted with 10 l Niskin bottles. Samples for biogenic silica $\delta^{30}Si$ analysis were generally collected at four depths between surface and ~200 m. For dissolved silicon $\delta^{30}Si$, samples were collected up to 15 depths in the upper 1000 m for the off-shelf water column and an additional sample taken at 2000 m.

We collected samples for silicon isotopic composition of $bSiO_2$ and $Si(OH)_4$ at seven stations (plateau: A3, B1, B5 and C1; off plateau: A11, B11 and C11; Fig. 1). Reference stations A3 and C11 were sampled twice at 18 and 10 days interval, respectively. Water samples were immediately filtered under pressure of filtered air through 0.4 μm porosity polycarbonate membranes (±1 to 4 l) using Perspex filtration units. Filtered seawater was stored in acid-cleaned polypropylene bottles at room temperature in the dark. Nuclepore membranes were stored in polycarbonate Petri dishes and dried overnight at 50 °C.

Samples were processed at a land-based laboratory (RMCA, Tervuren). The membranes for $bSiO_2$ were submitted to a wet-alkaline digestion (adapted from Ragueneau et al. (2005)) whereby $bSiO_2$ is dissolved with a 0.2 μmol l^{-1} NaOH solution (pH 13.3) at 100 °C for 40 min. As this digestion can also dissolve some lithogenic silica, we also analyzed aluminum (Al) in the digested solution to check for possible lithogenic contamination. Al in digested samples remained below the Inductively Coupled Plasma Atomic Emission Spectrometry detection limit of 0.05 ppm, while Si concentrations varied between 14 and 91 ppm. Using a Si:Al ratio of 3.74 for average crust (Taylor and McLennan, 1985), the lithogenic silica would reach less than 0.18 ppm in the digested samples. Considering $\delta^{30}Si$ signatures for clays to range from −2‰ to 0‰ (Basile-Doelsh, 2006) the maximum potential contribution of lithogenic Si appears to be negligible (Cardinal et al., 2007). Independent measurements by Mosseri et al. (2008) during KEOPS show the lithogenic contribution to the total particulate Si stock to average 7.3 ± 8.8%. One exception is station C1 located in shallow waters near Heard Island (Fig. 1) where the lithogenic fraction reached 32.2 ± 8.4%. However, at this station no samples were taken for $\delta^{30}Si_{bSiO_2}$. Furthermore, Ragueneau et al. (2005) report that during the first step of alkaline digestion – the only step we performed on KEOPS samples – all $bSiO_2$ and only a fraction of lithogenic silica were dissolved in agreement with the negligible lithogenic contamination for our samples.

$Si(OH)_4$ and $bSiO_2$ concentrations were measured on the same samples analyzed for Si-isotopic composition, via a colorimetric method (Grasshoff et al., 1983). Because $Si(OH)_4$ concentrations at stations A3, B1 and A11 were too low (<10 μmol l^{-1}) to directly apply the Si purification procedure required for Si-isotopic measurements (De La Rocha et al., 1996), a $Si(OH)_4$ preconcentration step was performed. This was achieved using a protocol adapted by Reynolds et al. (2006) from the MAGIC method (Karl and Tien, 1992): a two-step quantitative scavenging

of $Si(OH)_4$ by brucite [$Mg(OH)_2$] precipitate was obtained by adding 20 ml of 1 μmol l^{-1} NaOH per liter of seawater. The first precipitate was recovered by filtration (0.8 μm, polycarbonate membrane). To ensure complete Si-recovery a further 10 ml of NaOH 1 μmol l^{-1} was added to the filtrate, which was then filtered once more. These precipitates were subsequently redissolved in 15 ml HCl (3 μmol l^{-1}).

Silicon was precipitated and purified following the triethylamine molybdate co-precipitation method (De La Rocha et al., 1996). After combustion of the silicomolybdate precipitate in covered Pt crucibles, the pure cristobalite phase was transferred to pre-cleaned polypropylene vials. Dissolution of cristobalite was performed in a dilute HF/HCl mixture, as described in Cardinal et al. (2003).

Isotopic measurements were carried out on a Nu Plasma Multi-collector-Inductively Coupled Plasma Mass Spectrometer (MC-ICP-MS; ULB-RMCA, Brussels) using Mg external doping in dry plasma mode. Most of the Si-isotopic measurements [78% of $Si(OH)_4$ samples; 8% of $bSiO_2$ samples; and 55% of total samples] were performed following the methodology described by Cardinal et al. (2003). This method uses a low-resolution mode and cannot resolve the interference at ^{30}Si (mainly due to $^{14}N^{16}O$), and silicon isotopic signatures are measured as $\delta^{29}Si$ only. Following an upgrade of the Nu Plasma instrument, high resolution and pseudo high resolution were achieved, enabling the measurement of both $\delta^{29}Si$ and $\delta^{30}Si$, as described in Abraham et al. (2008). Results are discussed here using $\delta^{30}Si$ notation only. When only $\delta^{29}Si$ was measured, results were converted into $\delta^{30}Si$ using the theoretical conversion factor of 1.96 assuming a kinetic fractionation law (Young et al., 2002). Considering that Si uptake by diatoms is an enzymatic process (Hildebrand, 2008), the induced isotopic fractionation should follow a kinetic isotopic fractionation by analogy to C and N (François et al., 1993; Sigman et al., 2009). Diatoms drive the marine silicon cycle (Tréguer et al., 1995) and subsequently should control Si-isotopic distribution.

The precision and reproducibility (±2 standard deviations) of the measurements were ±0.10‰ ($\delta^{29}Si$) and ±0.15‰ ($\delta^{30}Si$). Accuracy of the measurements was checked on a daily basis using secondary reference material (Diatomite) whose Si-isotopic composition was characterized by an inter-comparison exercise (e.g., Reynolds et al., 2007).

3. Results

3.1. Hydrology and biogeochemical characteristics of the KEOPS area

During KEOPS, the different water masses characteristic of the summer Antarctic Zone (AZ) were present (Park et al., 1998a,b, 2008a; see Table 1 for a list of abbreviations). A relatively warm, fresh, well Mixed Layer (ML) capped the subsurface temperature minimum layer, referred to as winter water (WW). WW is a remnant of the former winter ML [hereinafter referred to as Antarctic Surface Water (AASW)]

Table 1
Abbreviation list.

HNLC	High Nutrient Low Chlorophyll
ACC	Antarctic Circumpolar Current
AZ	Antarctic Zone
APF	Antarctic Polar Front
AASW	Antarctic Surface Water
ML	Mixed Layer
WW	Winter Water
UCDW	Upper Circumpolar Deep Water
LCDW	Lower Circumpolar Deep Water
$^{30}\varepsilon$	fractionation factor
$\Delta^{30}Si$	apparent fractionation factor
f	relative silicon utilization
f_{UCDW}	UCDW contribution to a Si-pool
ΔSi	seasonal depletion
P	$bSiO_2$ production
D	$bSiO_2$ dissolution

that is capped by seasonal warming and freshening of the upper most surface waters, as shown by time-series observations at station KERFIX southwest of Kerguelen Island (Park et al., 1998a). Over the plateau, the geostrophic circulation is relatively sluggish and directed to the northwest following the local bathymetry (Fig. 1a, Park et al., 2008a). All stations were located south of the Antarctic Polar Front (APF) and separated from the direct influence of Kerguelen Island by a branch of this circumpolar jet (Fig. 1). The latter was characterized by low chlorophyll concentration (Mongin et al., 2008). However, mesoscale eddy activity at the APF could have sporadically advected waters from the north of the APF in the region of the northernmost stations (e.g., A11) (Mongin et al., 2008).

Based on the productivity criteria in Uitz et al. (2009), stations A1 to A3 and B1 to B5 were located within the bloom area (hereafter referred to as the fertilized bloom area). Off-shelf stations C11 and B11, as well as the stations in the South Eastern part of the plateau (C1–C7), were located within the HNLC area (Table 2). The remaining stations were in-between these two contrasting groups (e.g., A11). The fertilized bloom area was characterized by high primary and export production (Uitz et al., 2009; Savoye et al., 2008), as well as high $bSiO_2$ concentrations (Mosseri et al., 2008) (Table 2). A massive bloom was observed above the Kerguelen Plateau over the course of austral summer 2005 (Mongin et al., 2008). This bloom was almost exclusively composed of relatively large diatoms (Armand et al., 2008). The HNLC area contrasts the plateau region by low biogenic silica content, as well as by low primary and export production (Table 2) (Mosseri et al., 2008; Savoye et al., 2008; Uitz et al., 2009). The difference between the fertilized and HNLC areas was clearly observed in the chlorophyll section (Fig. 1b).

In the fertilized bloom area, low $Si(OH)_4$ concentrations coincided with high NO_3 concentrations, indicating a strong decoupling between both nutrients (Mosseri et al., 2008). On the other hand, the HNLC area had high concentrations of both $Si(OH)_4$ and NO_3 (Table 2).

3.2. Dissolved silicon

Profiles of $Si(OH)_4$ concentration and isotopic composition reveal a heavier isotopic composition in surface water, relative to deep waters, coinciding with a Si-depletion (Table 3; Fig. 2a,b). Similar conditions have been reported for the Atlantic, Southern and Pacific Oceans (De La Rocha et al., 2000; Cardinal et al., 2005; Reynolds et al., 2006; Beucher et al., 2008). Such vertical gradients are driven by diatom production combined with vertical mixing (Cardinal et al., 2005; Reynolds et al., 2006). For the different water masses identified by Park et al. (2008a), average $\delta^{30}Si_{Si(OH)_4}$ signatures were (Fig. 3f,g,h; Table 4): ML [0 to ~100 m], $+2.4 \pm 0.3$‰ (n = 23); WW [~100 to ~400 m], $+1.7 \pm 0.2$‰ (n = 32); Upper Circumpolar Deep Water (UCDW) [~400 to ~1400 m], $+1.3 \pm 0.2$‰ (n = 16); and Lower

Circumpolar Deep Water (LCDW) [~1400 to ~2600; sampling was performed only at 2000 m], $+1.1 \pm 0.2$‰ (n = 3).

These vertical variations of $\delta^{30}Si_{Si(OH)_4}$ were in good agreement with previous values reported for the AZ (Table 4; see Fig. 1 for the location of these studies), indicating wide spatial biogeochemical uniformity for this zone regarding the silicon cycle. Notwithstanding this uniformity, a clear seasonality can be discerned in the surface waters. The summer ML $\delta^{30}Si_{Si(OH)_4}$ values in the present study ($+2.4 \pm 0.3$‰ = average of the fertilized bloom and HNLC areas), as well as the summer values for the Atlantic EIFEX expedition ($+2.6 \pm 0.1$‰ outside the fertilized patch; Cavagna et al., in press), were heavier than the spring values reported for the Australian sector: $+1.9 \pm 0.1$‰ (Cardinal et al., 2005). This is consistent with the ML becoming more depleted in $Si(OH)_4$ with progress of the growth season, yielding to an enrichment of the $Si(OH)_4$ pool in ^{30}Si, owing to preferential ^{28}Si uptake by diatoms and their export. This type of seasonal concentration and isotopic effect has also been observed in the Pacific sector by Varela et al. (2004) during a bloom that was propagating from the APF southward through the AZ.

The ML at stations A3-1, A3-2, and B1 in the fertilized bloom area had lower $Si(OH)_4$ concentrations (on average 2.1 μmol l^{-1}) and heavier $\delta^{30}Si_{Si(OH)_4}$ values ($+2.5$‰ to $+2.7$‰) as compared to off-shelf stations (Figs. 2a,b and 3b,f). Station B5, located at the edge of a $Si(OH)_4$ gradient between A3 and C11, was an exception. It had a higher $Si(OH)_4$ concentration, reaching 13.9 μmol l^{-1}, but had $\delta^{30}Si_{Si(OH)_4}$ values similar to those in the fertilized bloom area (A3 and B1). Mosseri et al. (2008) observed the highest biogenic silica production rates at station B5, while $bSiO_2$ production rates at A3 were low and similar to those at station C11 (Mosseri et al., 2008). This situation probably reflects the shift of the bloom from A3 to the more Si-replete areas around B5, that was reported from satellite observations (Mongin et al., 2008) and predicted by a phytoplankton class-specific primary production model (Uitz et al., 2009). Site B5 thus appears to show different characteristics from the fertilized bloom area (A3 and B1), and therefore was excluded from the mass and isotopic balance calculations for the latter (Section 4.4.3).

The low production HNLC stations C11-1, C11-2 and B11 (Uitz et al., 2009) were characterized by high ML $Si(OH)_4$ concentrations (on average 27.2 μmol l^{-1}) and lighter $\delta^{30}Si_{Si(OH)_4}$ ($+2.1$ to $+2.3$‰) (Figs. 2a,b and 3b,f). In contrast to the HNLC conditions, site A11 had the heaviest ML $\delta^{30}Si_{Si(OH)_4}$ ($+2.8 \pm 0.1$‰) coinciding with near complete Si-depletion (4.6 ± 2.6 μmol l^{-1}). The occurrence of such a heavy isotopic signature fits with an advection of Si-depleted water from north of the APF that is associated with heavier $\delta^{30}Si_{Si(OH)_4}$ (Varela et al., 2004; Cardinal et al., 2005) and was in agreement with observed mesoscale eddy activity associated with the APF (Mongin et al., 2008). The low productivity station C1 (Uitz et al., 2009) at the southern end of the plateau had a lighter $\delta^{30}Si_{Si(OH)_4}$ ($+1.9$‰) than for the HNLC area, but a similar $Si(OH)_4$ concentration (26.6 μmol l^{-1}).

Table 2
Biogeochemical properties during KEOPS.

	Stations	$Si(OH)_4$ μmol l^{-1}	NO_3[a] μmol l^{-1}	Mixed layer depth[b] m	Primary production[c] g C m^{-2} d^{-1}	$bSiO_2$ standing stock[d] mmol m^{-2}	Export production (EP)[e] mg C m^{-2} d^{-1}
Fertilized area	A1–5 B1–B5	2.1	23.0	70–100	~1	1100 ± 600	222
HNLC area	B9–B11 C transect	27.2	29.4	70–100	~0.3	350 ± 100	85

[a] Autoanalyzer onboard.
[b] From Park et al. (2008a).
[c] Integrated over the euphotic layer (from Uitz et al. (2009)).
[d] Integrated from 0 to 200 m (from Mosseri et al. (2008)).
[e] Export at 125 m (from Savoye et al. (2008)).

Table 3

Si(OH)$_4$ and bSiO$_2$ concentrations and isotopic compositions. The ML for A11 and A3 repeat represents two merged depths for Si(OH)$_4$. Only the standard deviations for duplicates are shown.

Station	Depth	Si(OH)$_4$	$\delta^{30}Si_{Si(OH)_4}$	bSiO$_2$	$\delta^{30}Si_{bSiO_2}$
	m	µmol L^{-1}	‰ ± 2SD	µmol L^{-1}	‰ ± 2SD
A11-CTD 11	8–76	3.6	2.78 ± 0.12	n.a.	n.a.
20/01/2005	8	3.3	n.a.	1.3	n.a.
49.09°S–74.00°E	30	2.8	n.a.	2.0	2.04 ± 0.15
	76	4	n.a.	2.5	1.91 ± 0.13
	102	8.4	n.a.	2.1	n.a.
	126	22.3	2.08	2.3	1.71 ± 0.14
	151	32.2	2.01 ± 0.15	6.3	1.03 ± 0.16
	201	41.5	1.62		
	202	50.8	1.73 ± 0.13		
	353	61.4	1.31		
	403	65.7	1.52		
	504	74.8	1.03		
	655	79.1	1.41 ± 0.16		
	807	82.9	1.37		
	2020	108.0	1.34 ± 0.13		
B11-CTD 50	11	25.9	2.30 ± 0.08	1.5	n.a.
28/01/2005	52	25.1	2.18 ± 0.13	1.6	1.24 ± 0.14
50.30°S–76.60°E	76	25.4	2.14 ± 0.21	2.0	1.12 ± 0.16
	101	31.6	2.26	2.9	1.08 ± 0.02
	125	42.0		1.3	n.a.
	151	42.7	1.68	n.a.	n.a.
	201	51.0	1.54	1.3	1.17 ± 0.11
	252	62.5	1.37		
	302	67.5	1.46		
	403	78.1	1.37		
	504	77.7	1.23 ± 0.20		
	654	83.1	1.41		
	805	90.4	1.10		
	2025	115.0	0.97		
C11-CTD 42	9	25.9	2.28	1.8	0.89
26/01/2005	49	25.4	2.30	2.7	1.24 ± 0.21
51.37°S–77.57°E	76	27.3	2.39	3.0	1.00 ± 0.11
	99	30.6	2.12	2.4	1.13 ± 0.13
	125	40.0	n.a.	1.1	n.a.
	151	41.7	1.69	0.9	n.a.
	201	54.4	1.41		
	252	59.5	1.41		
	304	68.6	1.51		
	353	74.6	1.37		
	404	80.3	1.35		
	504	82.1	1.26		
	555	81.8	1.21		
	656	89.8	1.26		
	807	90.6	1.42		
	2022	111.0	0.91		
C11R-CTD 83	11	25.7	2.14	1.5	1.44 ± 0.12
5/02/2005	51	26.8	2.30	1.5	n.a.
51.37°S–77.57°E	74	27.4	1.93	2.1	1.16
	100	29.1	1.97	1.4	1.08 ± 0.10
	151	43.5	1.56	0.7	0.98 ± 0.15
	202	55.2	1.56		
	303	75.2	1.52		
A3-CTD 32	10	1.2	n.a.	3.1	2.08 ± 0.02
23/01/2005	31	n.a.	n.a.	2.4	2.49 ± 0.22
50.38°S–72.05°E	51	1.4	n.a.	3.5	n.a.
	75	2.2	n.a.	5.0	2.14 ± 0.10
	101	4.7	n.a.	6.0	1.96 ± 0.12
	124	16.3	n.a.	9.5	1.78 ± 0.12
	151	17.4	2.09		
	201	30.2	1.80		
	302	48.4	1.79		
	352	56.0	1.50		
	403	61.6	1.34		
A3R-CTD 119	12–52	1.3	2.51	n.a.	n.a.
12/02/2005	12	1.3	n.a.	1.4	2.42 ± 0.16
50.38°S–72.05°E	30	1.3	n.a.	1.9	n.a.
	52	1.4	n.a.	1.9	2.26 ± 0.15
	75	4.2	n.a.	2.9	n.a.
	151	18.7	2.10		
	202	31.3	2.22 ± 0.14		
	353	50.6	1.64		

Table 3 (continued)

Station	Depth	Si(OH)$_4$	$\delta^{30}Si_{Si(OH)_4}$	bSiO$_2$	$\delta^{30}Si_{bSiO_2}$
	m	µmol L^{-1}	‰ ± 2SD	µmol L^{-1}	‰ ± 2SD
B1-CTD 68	3	2.3	n.a.	3.4	n.a.
2/02/2005	51	2.4	2.67 ± 0.09	4.1	2.40 ± 0.13
51.30°S–73.00°E	75	3.5	n.a.	4.2	2.23 ± 0.11
	100	10.6	1.94 ± 0.13	4.3	1.96 ± 0.14
	127	22.3	2.00 ± 0.07		
	153	27.8	1.94 ± 0.14		
	201	41.0	1.77 ± 0.15		
	300	50.1	1.87 ± 0.08		
B5-CTD 60	11	12.2	2.42	3.0	1.70 ± 0.15
30/01/2005	52	12.1	2.68 ± 0.14	3.3	1.55 ± 0.12
51.06°S–74.36°E	77	17.3	2.55	2.2	n.a.
	100	21.1	2.12	1.4	1.65 ± 0.12
	151	33.7	1.68	1.3	1.57 ± 0.12
	201	39.1	1.87	1.7	n.a.
	252	45.8	1.70		
	352	59.7	1.30		
	404	70.9	1.33		
	456	71.0	1.30		
C1-CTD 100	10	27.2	1.83		
8/02/2005	50	25.7	1.95		
53.11°S–72.52°E	103	25.7	2.08 ± 0.09		
	132	28.1	2.02 ± 0.02		

This shallow station (bottom depth 150 m) was located close to Heard Island, and the ML reached the underlying basalt floor. Knowing that ocean island basalts have a $\delta^{30}Si_{Si(OH)_4}$ of -0.4 ± 0.1‰ (Douthitt, 1982; Georg et al., 2007) the light isotopic composition of dissolved silicate at C1 could reflect a significant contribution of basalt alteration into the ML Si(OH)$_4$ pool. Based on a Montecarlo simulation (normal distribution, n = 1000) with ocean island basalts and HNLC-ML as $\delta^{30}Si$ end-members, we estimate this contribution at $10 \pm 5\%$ (i.e., 2.6 ± 1.3 µmol l^{-1}). Selecting either HNLC or C1 ML end-member Si(OH)$_4$ concentration does not affect the outcome of the previous calculation. Based on the Nd isotopic balance calculation Jeandel et al. (submitted for publication) identified basalt alteration process at C1 that should supply significant lithogenic fluxes of elements Si, Mg, Ca, Fe to the ML. For Si, such contribution could be 2 to 3 µmol l^{-1} (C. Jeandel, pers. comm., 2010) which is similar to our estimate. We are unable to determine the contribution of this basalt end-member with better precision because (1) a limited number of samples were collected and (2) the Si-isotopic fractionation factor associated with weathering process is largely unknown (Ziegler et al., 2005). Furthermore, advection from southern AASW which is likely to have a lower $\delta^{30}Si_{Si(OH)_4}$ signature (Varela et al., 2004; Cardinal et al., 2005) could also be significant at this southernmost C1 station (Fig. 1a). Overall we conclude that the silicon signatures at the A11 and C1 sites are intermediate between those for the fertilized and the HNLC areas and therefore were not taken into account in the mass and isotopic balance calculations for the HNLC area (C11 and B11; Section 4.3.2).

The ML in the fertilized bloom and HNLC areas exhibited significantly different $\delta^{30}Si_{Si(OH)_4}$ signatures, reflecting different degrees of Si-utilization by diatoms, which were dominant throughout KEOPS (Armand et al., 2008). A trend in the WW (100–400 m) composition between the fertilized bloom and the HNLC waters (Table 4 and Fig. 3c,g) was also observed, with the former having a lower Si(OH)$_4$ concentration (34.2 µmol l^{-1}) and a heavier $\delta^{30}Si_{Si(OH)_4}$ composition (+1.9‰), while the latter showed a higher Si(OH)$_4$ concentrations and lighter isotopic signature (52.5 µmol l^{-1} and +1.5‰).

3.3. Biogenic silica

The fertilized bloom ML region showed heavier $\delta^{30}Si_{bSiO_2}$ signatures than the HNLC region, similar to the dissolved $\delta^{30}Si_{Si(OH)_4}$ observations (+2.3 ± 0.1‰ vs. +1.1 ± 0.1‰, respectively) (Figs. 2c,d and 3a,e;
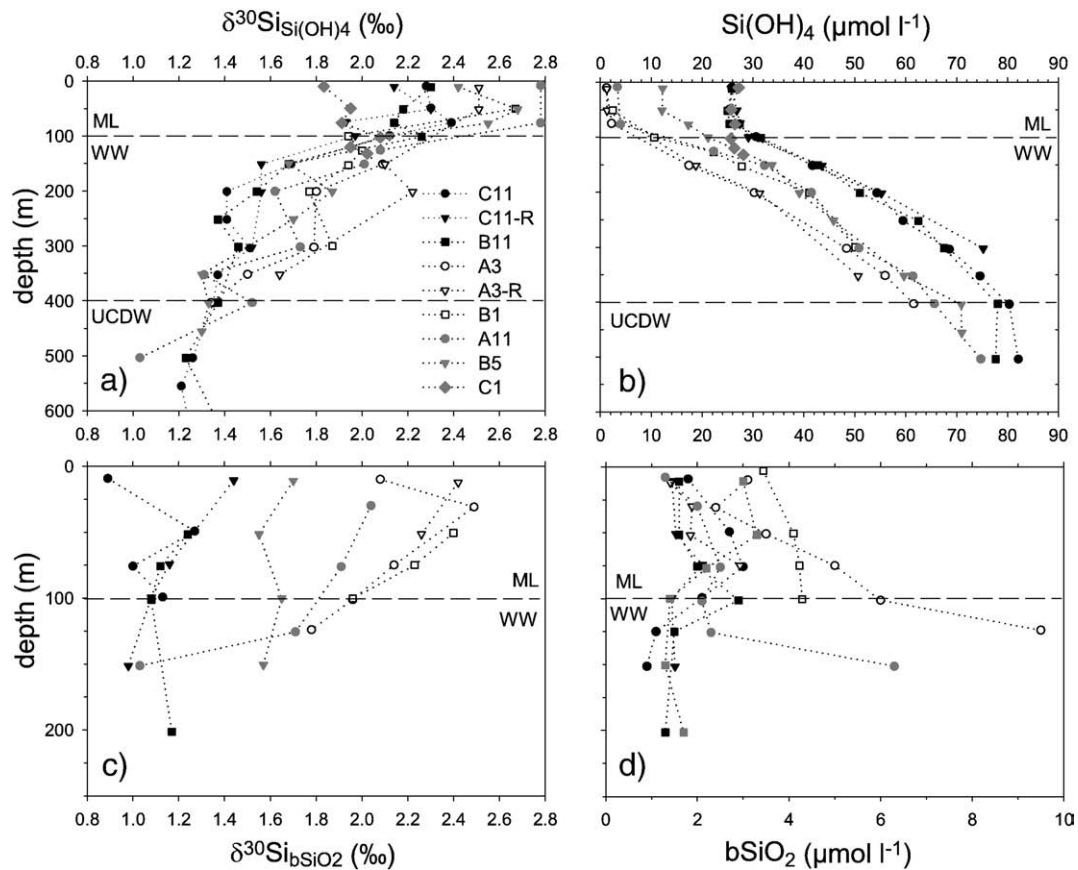
Fig. 2. Upper 550 m profiles for the stations characteristic of the fertilized (plateau) bloom area (white symbols), HNLC area (black symbols), and the three intermediates stations, A11 (grey dots), B5 (grey triangles) and C1 (grey diamonds). (a) $\delta^{30}Si_{Si(OH)_4}$, (b) $Si(OH)_4$ concentrations, (c) $\delta^{30}Si_{bSiO_2}$, and (d) $bSiO_2$ concentrations. The first two points for $\delta^{30}Si_{Si(OH)_4}$ of A11 and A3 are values for merged samples. The horizontal dashed lines represent the limit of the different water masses.

Table 4). Stations A11 and B5 had intermediate ML Si-isotopic compositions ($+2.0 \pm 0.1\permil$ and $+1.6 \pm 0.1\permil$, respectively), as well as $Si(OH)_4$.

$\delta^{30}Si_{bSiO_2}$ values were systematically lighter than $\delta^{30}Si_{Si(OH)_4}$, in agreement with the preferential uptake of light Si-isotopes by diatoms (De La Rocha et al., 1997; Milligan et al., 2004; Varela et al., 2004;
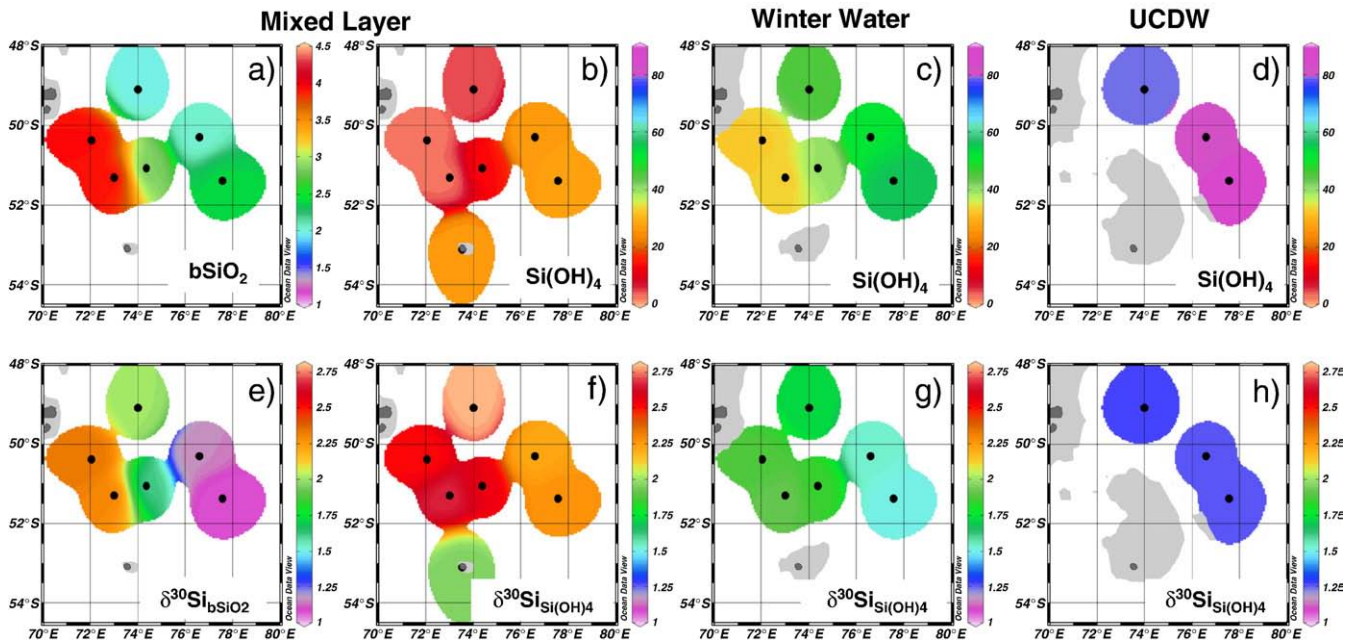
Fig. 3. $\delta^{30}Si$ and Si distribution in mixed layer (a,b,e,f), Winter Water (c,g), and Upper Circumpolar Deep Water (d,e). The values are the mean of the different water masses (defined by Park et al. (2008a)) at each station. Caution has to be taken for the values extrapolated owing the poor sampling coverage. The bathymetry is scaled at 50 m for ML, 250 m for WW, and 600 m for UCDW.

Table 4
Average $\delta^{30}Si_{Si(OH)_4}$, and $\delta^{30}Si_{bSiO_2}$ for different water masses of the Antarctic Zone (± 1 SD). ML: Mixed Layer; WW: Winter Water; UCDW: Upper Circumpolar Deep Water; LCDW: Lower Circumpolar Deep Water. See Fig. 1a for the locations of these studies. Except for AESOPS and SOFex, the area averages and error bars were calculated based on the mean values for each station. For AESOPS and SOFex, the area averages and error bars were calculate for the whole dataset south of APF.

	Si(OH)$_4$	KEOPS[a]		EIFEX[b]	CLIVAR SR3[c]	AESOPS[d]	SOFeX[d]
		Plateau	Out plateau	Out patch			
ML	$\delta^{30}Si_{Si(OH)_4}$ (‰)	2.6 ± 0.2	2.2 ± 0.2	2.6 ± 0.1	1.8 ± 0.2	2.5 ± 0.9	2.1 ± 0.7
	Si(OH)$_4$ (µmol l^{-1})	2.1 ± 0.6	27.2 ± 0.2	10.3 ± 2.4	28.5 ± 0.5	50 to <10	60 to <10
WW	$\delta^{30}Si_{Si(OH)_4}$ (‰)	1.9 ± 0.1	1.5 ± 0.0	1.6 ± 0.2	1.3 ± 0.2		
	Si(OH)$_4$ (µmol l^{-1})	34.2 ± 1.9	52.5 ± 3.3	37.3 ± 2.8	60.9 ± 9.3		
UCDW	$\delta^{30}Si_{Si(OH)_4}$ (‰)			1.3 ± 0.2	1.3 ± 0.1		
	Si(OH)$_4$ (µmol l^{-1})	78.4 ± 8.5		75.5 ± 3.2	89.8 ± 8.8		
LCDW	$\delta^{30}Si_{Si(OH)_4}$ (‰)	1.1 ± 0.2			1.1		
	Si(OH)$_4$ (µmol l^{-1})	111.3 ± 3.5	1.3 ± 0.2		117.2		
	bSiO$_2$						
ML	$\delta^{30}Si_{bSiO_2}$ (p.mil)	2.3 ± 0.1	1.2 ± 0.2	1.5 ± 0.4	0.8 ± 0.2	1.2 ± 2.1	1.0 ± 1.6
under ML		1.9 ± 0.1	1.0 ± 0.1		0.7 ± 0.2		

[a] This study, January–February 2005.
[b] Cavagna et al. (in press), January–March 2004.
[c] Cardinal et al. (2005), 1 profile (61°S), November 2001.
[d] Varela et al. (2004), AESOPS October 1997–March 1998, SOFeX January–February 2002.

Alleman et al., 2005; Cardinal et al., 2007) (Fig. 3a,b,e,f; Tables 3 and 4). The average ML $\Delta^{30}Si$ value [$\Delta^{30}Si = \delta^{30}Si_{bSiO_2} - \delta^{30}Si_{Si(OH)_4}$] in the fertilized area (-0.3 ± 0.1‰) was much lower than in the HNLC area (-1.0 ± 0.2‰), with B5 and A11 (-0.9 and -0.8‰, respectively) again displaying intermediate values which were closer to the HNLC values.

For the fertilized area and A11, we observed a gradient toward lighter bSiO$_2$ isotopic composition with increasing depth. These stations had a deep bSiO$_2$ maximum in the subsurface (125–150 m; Fig. 2c,d). Cardinal et al. (2007) also reported a decrease in $\delta^{30}Si_{bSiO_2}$ between ML to underlying waters for the polar frontal zone in the Australian sector, while no such feature was observed in the AZ. Below the ML, the $\delta^{30}Si_{bSiO_2}$ was lighter than the corresponding $\delta^{30}Si_{Si(OH)_4}$ by 0.5‰ (B11 and C11), 0.3‰ (B5), 0.0‰ (B1), and 0.7‰ (A11) (Fig. 2a,c). Such differences were too low to be explained only by *in situ* growth of diatoms and are in agreement with the fact that, at the time of sampling, diatoms below the ML mainly represented either accumulated diatoms that settled out from the surface waters (Mosseri et al., 2008; Uitz et al., 2009) or a mixture of settled and *in situ* grown diatoms.

$\delta^{30}Si_{bSiO_2}$ values presented here were on the heavy side of the reported range for the AZ (Table 4). This reflects the fact that the growth season was already well advanced during KEOPS, with maximal Si(OH)$_4$ depletion (Brzezinski et al., 2001; Quéguiner and Brzezinski, 2002) and associated enrichment in heavy Si-isotopes of the particulate and dissolved Si-phases (Varela et al., 2004).

4. Discussion

4.1. General considerations

The fractionation of Si isotopes during biological production by diatoms can be described using simple closed or open system models (De la Rocha et al., 1997; Sigman et al., 1999). The Rayleigh model (or closed system model) assumes that nutrient consumption is not replenished by external sources and describes the evolution of the isotopic signatures of Si(OH)$_4$ (Eq. (1)), instantaneous bSiO$_2$ (Eq. (2)) and accumulated bSiO$_2$ (Eq. (3)):

$$\delta^{30}Si_{Si(OH)_4} = \delta^{30}Si_{Si(OH)_4 \, initial} + {}^{30}\varepsilon \cdot \ln(f) \tag{1}$$

$$\delta^{30}Si_{bSiO_2 inst} = \delta^{30}Si_{Si(OH)_4} + {}^{30}\varepsilon \tag{2}$$

$$\delta^{30}Si_{bSiO_2 acc} = \delta^{30}Si_{Si(OH)_4 initial} - {}^{30}\varepsilon \cdot \frac{f \cdot \ln(f)}{1 - f} \tag{3}$$

In Eqs. (1) and (3), f is defined as:

$$f = \frac{[Si(OH)_4]_{observed}}{[Si(OH)_4]_{initial}} \tag{4}$$

The alternative to the Rayleigh model is the steady state, or open flow-through system model, where Si(OH)$_4$ is supplied and partially consumed. The supply of Si(OH)$_4$ equals the sum of gross biogenic silica production and loss of residual Si(OH)$_4$ by advection. The evolution of the isotopic signatures in such system is as follows:

$$\delta^{30}Si_{Si(OH)_4} = \delta^{30}Si_{Si(OH)_4 initial} - {}^{30}\varepsilon \cdot (1 - f) \tag{5}$$

$$\delta^{30}Si_{bSiO_2} = \delta^{30}Si_{Si(OH)_4 initial} + {}^{30}\varepsilon \cdot f = \delta^{30}Si_{Si(OH)_4} + {}^{30}\varepsilon \tag{6}$$

$$\Delta^{30}Si = \delta^{30}Si_{bSiO_2} - \delta^{30}Si_{Si(OH)_4} \tag{7}$$

$\Delta^{30}Si$ equals ${}^{30}\varepsilon$ in case the open system mode applies, but also in case $\delta^{30}Si_{bSiO_2}$ represents instantaneous bSiO$_2$ in the Rayleigh model approach (Eq. (2)). The implied absence of bSiO$_2$ accumulation in the steady state model represents an oversimplification of the true conditions, since the bSiO$_2$ pool likely consists of a mixture of detrital and living cells, especially toward the end of the productive period (Brzezinski et al., 2003; Beucher et al., 2004). The Rayleigh model only describes two extreme ideal situations: any bSiO$_2$ present is the result of an instantaneous production and will be exported from the system (Eq. (2)) or reflects accumulated, non-sinking bSiO$_2$ (Eq. (3)). Clearly, reality is lying in-between these two extremes.

The evolution of $\delta^{30}Si_{Si(OH)_4}$ vs. [Si(OH)$_4$], as described by the Rayleigh and steady state models, follows a curved or a straight line, respectively.

Demarest et al. (2009) report an isotopic fractionation (${}^{30}\varepsilon = -0.55$‰) associated with dissolution of bSiO$_2$. By increasing the euphotic bSiO$_2$ dissolution:production ratio (D:P), the resulting fractionation factor associated with Si uptake and dissolution would be as follows:

$$ {}^{30}\varepsilon_{tot} = {}^{30}\varepsilon_{upt} + \frac{D}{P} \cdot {}^{30}\varepsilon_{diss} \tag{8}$$

where $^{30}\varepsilon_{upt}$ is the isotopic fractionation factor associated with $bSiO_2$ production, and ε_{diss} the one associated with $bSiO_2$ dissolution. Although $bSiO_2$ production and dissolution occur simultaneously in marine surface waters, for a given diatom cell these processes are uncoupled temporally since it is not until after diatom death and degradation of its protective organic coating that the diatom frustule starts to dissolve (Bidle and Azam, 1999). Such decoupling is not taken into account in Eq. (8) which assumes steady state with no $bSiO_2$ accumulation. Additional studies that combine $\delta^{30}Si_{bSiO_2}$ analysis with measurements of $bSiO_2$ production and dissolution rates have potential to reveal how the silicon isotope distribution is affected by the fractionation of silicon isotopes during $bSiO_2$ dissolution (Demarest et al., 2009).

4.2. Estimation of the fractionation factor

In order to limit possible bias on local $^{30}\varepsilon$ estimates due to intense mixing above the plateau and difficulties in selecting the appropriate Si-source (see Section 4.4) we only used the data for the HNLC off-plateau region to estimate $^{30}\varepsilon$. A further reason for focusing on the HNLC area only is that here $bSiO_2$:$Si(OH)_4$ concentration ratios were much lower than in the fertilized bloom area (Tables 2 and 4) thereby reducing the possible impact of $bSiO_2$ dissolution on the $Si(OH)_4$ isotopic signal in the ML. Using the WW $Si(OH)_4$ pool as the Si-source (cf. Section 4.3.1), we calculated $^{30}\varepsilon$ values of -1.0 ± 0.3‰ and -1.3 ± 0.2‰, for the Rayleigh and steady state models (Eqs. (1) and (5)), respectively, for the HNLC area.

To date, only four *in situ* studies have estimated the fractionation factor in the ACC, with following reported $^{30}\varepsilon$ values: -1.5 ± 0.3‰ (Varela et al., 2004), -0.9 ± 0.3‰ (Cardinal et al., 2005), -1.3 ± 0.4‰ (Cardinal et al., 2007), and -1.4 ± 0.1‰ (Cavagna et al. in press). Our estimates are not significantly different from these literature values. The relatively large variability in the fractionation factor estimates probably results from the difficulty in accurately determining Si-source(s) and from the mixing of waters with silicic acid pools that have experienced different degrees of biological consumption (Cardinal et al., 2005; Reynolds et al., 2006; Beucher et al., 2008). The fractionation factor estimates reported in Cardinal et al. (2007) and Cavagna et al. (in press) actually represent apparent fractionations or $\Delta^{30}Si$. Since $\delta^{30}Si_{bSiO_2}$ is set by processes which may not be contemporaneous with those setting $\delta^{30}Si_{Si(OH)_4}$ (Cardinal et al., 2007; Demarest et al., 2009), we decided not to include these estimates when calculating an average $^{30}\varepsilon$ for the ACC region, even though variations between different $^{30}\varepsilon$ values were not significant. The average $^{30}\varepsilon$ value obtained for the ACC then becomes -1.2 ± 0.2‰ (from this study, Cardinal et al. (2005) and $\delta^{30}Si_{Si(OH)_4}$ from Varela et al. (2004)), which is indistinguishable of the value obtained from *in vitro* incubations under tropical to temperate conditions (-1.1 ± 0.4‰, De la Rocha et al., 1997).

4.3. Si-isotopic constraints in the HNLC area

4.3.1. Silicon isotopes dynamics

As discussed in Section 3.2, the HNLC area is defined with stations B11 and C11. Fig. 4a shows the isotopic fractionation trends due to Si uptake resulting from the models, taking WW as the Si-source and using the average ACC $^{30}\varepsilon$ of -1.2 ± 0.2‰ discussed in the previous section. The observed ML $\delta^{30}Si_{Si(OH)_4}$ fall along these trends (Fig. 4a), in agreement with the seasonal evolution of the ML. Because WW is the remnant of the former winter ML [also referred to as Antarctic Surface Water (AASW)], it represents the initial conditions prevailing before the summer stratification (Park et al., 1998a, 1998b) and the start of the bloom. Pondaven et al. (2000) have shown that this is the case for the AZ in the Indian sector, with early summer/late winter surface ocean $Si(OH)_4$ contents being less than 7% different from WW $Si(OH)_4$ concentrations. Such a small difference has an undetectable
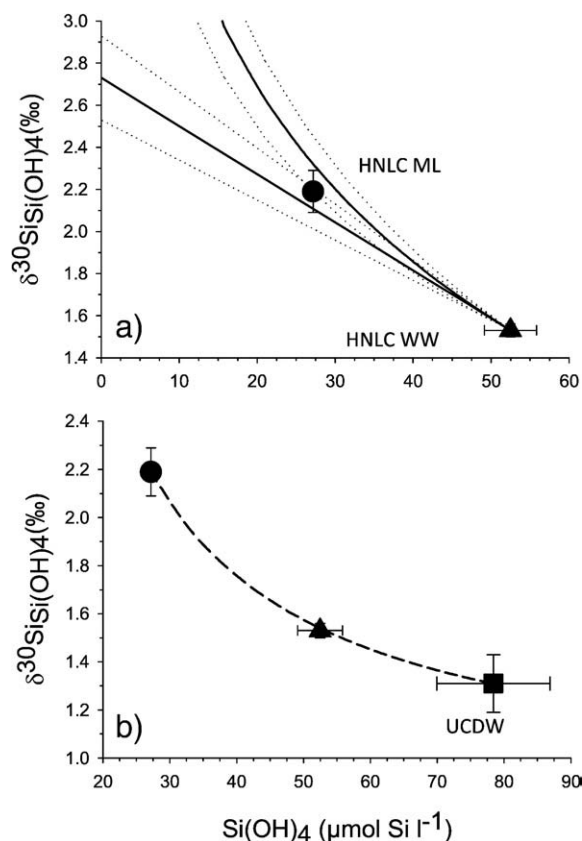
Fig. 4. $\delta^{30}Si_{Si(OH)_4}$ vs. $[Si(OH)_4]$ for the different Si-pools in the HNLC area (±1 SD; stations B11 and C11) during KEOPS: (a) fractionation trends following the steady state (straight line) or Rayleigh (curved line) models calculated with HNLC WW as the Si-source and an average ACC fractionation factor of -1.2 ± 0.2‰; (b) mixing curves between HNLC-ML and UCDW. The black circle, triangle and square represent ML, WW, and UCDW, respectively. The area averages and error bars were calculated based on the mean values for each station.

impact on $\delta^{30}Si_{Si(OH)_4}$. Therefore, for the HNLC area, it seems reasonable to consider the prevailing WW Si-pool characteristic conditions of the initial ones. Average WW $Si(OH)_4$ concentration and isotopic compositions were 52.5 ± 3.3 µmol l^{-1} and $+1.5\pm0.0$‰, respectively (Table 4).

Fig. 4a shows that Si-utilization in the KEOPS HNLC area was not large enough to allow resolving the steady state and Raleigh operational modes. However, a strictly closed system mode of operation for the ML Si-pool is unlikely because high internal tide activity associated with the plateau is likely to propagate toward the surrounding HNLC areas (Park et al., 2008b) increasing turbulent diffusion and vertical mixing. Therefore, a steady state mode, or at least a combination of Rayleigh and steady state modes which depends on a seasonally variable ratio of Si-supply vs. uptake, is more likely.

Taking the average ACC $^{30}\varepsilon$ value (see Section 4.2) and the HNLC WW as Si-source, the steady state (Eq. (6)) and Rayleigh models (Eq. (2)) yield a $\delta^{30}Si_{bSiO_2}$ of $+1.0$‰ which is not significantly different from the observed value of $+1.1\pm0.2$‰ (Table 4). Note that in the case of the Rayleigh model the calculated $^{30}Si_{bSiO_2}$ value is for instantaneous $bSiO_2$. The theoretical $\delta^{30}Si$ value of accumulated $bSiO_2$ (Eq. (3)) should be $+0.7$‰, which is significantly lighter than the one observed and indicates significant previous export of $bSiO_2$ carrying lighter $\delta^{30}Si$. However, dissolution of $bSiO_2$ would also have enriched remnant $bSiO_2$ in ^{30}Si (Demarest et al., 2009). From the above discussion it appears difficult to pin down the true processes and the small differences between $\delta^{30}Si_{bSiO_2}$ of theoretical and observed values preclude to go further into the interpretation.

4.3.2. Silicon mass balance

The KEOPS cruise took place during the senescent phase of the bloom, at the end of the growth season (Blain et al., 2007; Mosseri et al., 2008; Mongin et al., 2008). In the following section we therefore considered the summer ML conditions to reflect the conditions before overturning ended the stratification. This hypothesis is in agreement with the two repeat C11 stations showing no variation. ML and UCDW can thus be considered end-members, which will generate a homogenous layer in the upper 400 m constituting AASW as a result of convective mixing at the onset of winter (Park et al., 2008a). Fig. 4b shows it is the case since WW falls on a mixing curve between the HNLC-ML and UCDW waters calculated by the following equation:

$$m_{AASW} \cdot \delta^{30}Si_{AASW} = m_{UCDW} \cdot \delta^{30}Si_{UCDW} + m_{HNLC-ML} \cdot \delta^{30}Si_{HNLC-ML} \tag{9}$$

where m_{UCDW} and $m_{HNLC-ML}$ represent the Si contributions of UCDW and HNLC-ML:

$$m_{AASW} = m_{UCDW} + m_{HNLC-ML} \tag{10}$$

and the relative UCDW Si contribution (f_{UCDW}) to AASW is defined as:

$$f_{UCDW} = \frac{m_{UCDW}}{m_{AASW}}. \tag{11}$$

Combining Eqs. (9) and (11) gives:

$$f_{UCDW} = \frac{\delta^{30}Si_{AASW} - \delta^{30}Si_{HNLC-ML}}{\delta^{30}Si_{UCDW} - \delta^{30}Si_{HNLC-ML}}. \tag{12}$$

Using Eq. (12) we estimated that the UCDW contributed $78 \pm 12\%$ of the $Si(OH)_4$ standing stock of the HNLC AASW as a result of this mixing. Standard errors for the different mass balance estimations were obtained from Montecarlo simulations (Normal distribution, n = 1000).

Integrating the observed WW $Si(OH)_4$ concentration over the whole water layer between surface and WW (i.e., integrating over the 400 m AASW winter layer; Park et al., 2008a) and multiplying that amount with f_{UCDW}, we obtain that UCDW contributes 16.0 ± 2.8 mol Si m^{-2} to AASW. The 100 m deep summer ML will thus inherit $(100/400) \times (16.0 \pm 2.8)$ or 4.0 ± 0.7 mol Si m^{-2} yearly at the start of the growth season each overturning event (that is once per year). Assuming steady state conditions to apply (supply equaling export) at the annual scale, the effective annual net bSiO$_2$ production should equal the annual vertical UCDW Si-supply of 4.0 ± 0.7 mol Si m^{-2} yr^{-1}.

The mass balance yielded a seasonal $Si(OH)_4$ depletion [= ΔSi; difference between initial (= HNLC WW) and final ML $Si(OH)_4$ concentration] integrated over the mixed layer (0–100 m) of 2.5 ± 0.2 mol Si m^{-2} yr^{-1}, which is 1.5 ± 0.7 mol Si m^{-2} yr^{-1} less than the annual net bSiO$_2$ production calculated above. Net bSiO$_2$ production should represent the sum of ΔSi + vertical Si-supply + Si-advection. Thus, the imbalance between seasonal $Si(OH)_4$ depletion and net bSiO$_2$ production should give an estimate of the summertime Si-supply, either vertically or horizontally by advection. Since (1) the ACC fronts delimit zones with relatively constant hydrological and biogeochemical properties (Tréguer and Jacques, 1992; Sokolov and Rintoul, 2007) and (2) water particles spend several years in each zone and therefore take part in several winter convective mixings (S. Speich, pers. comm. 2009), we can thus consider that a water parcel in the Antarctic Zone is surrounded by water with relatively similar properties and subject to the same seasonal evolution. It thus seems appropriate to construct mass and isotopic balances at an annual scale, using a simple 1-D approach. Since advective Si-supply can then be neglected, the imbalance between annual net bSiO$_2$ production (equal to the UCDW vertical supply) and seasonal

depletion (i.e., 1.5 ± 0.7 mol Si m^{-2}) represents the summertime Si-supply via vertical turbulent diffusion processes. While we are confident that our mass balance description is valid for the AZ HNLC area, it appears not to be applicable for the productive Kerguelen Plateau waters surrounded by waters with relatively low productivity. For the plateau area, advection from the surrounding areas seems necessary to close mass and isotopic balances (see further below, Section 4.4.3).

Our estimated annual net bSiO$_2$ production values slightly exceed the range of published net bSiO$_2$ production values for the AZ (2.4 to 3.3 mol Si m^{-2} yr^{-1}; Pondaven et al., 2000; Nelson et al., 2002; Pollard et al., 2006), but are not significantly different. Using an inverse modeling approach for nutrient distributions, Jin et al. (2006) estimated opal export out of the euphotic layer in the Indian sector of the Southern Ocean in the range of 1 to 7 mol Si m^{-2} yr^{-1}, which encompasses our estimate of net bSiO$_2$ production. The presence of a productive spot east to the Kerguelen Plateau is recognized by Jin et al. (2006) and is confirmed by remote sensing chlorophyll data presented by Sokolov and Rintoul (2007). The latter authors report that most regions of elevated chlorophyll in the open Southern Ocean can be explained by upwelling of nutrients (both macro- and micro-nutrients) at sites where the ACC interacts with topography, followed by downstream advection. Recurrent blooms downstream of islands and bathymetric features as is the case for the Kerguelen area HNLC area (Fig. 1b) fit to this scenario.

4.4. Si-isotopic constraints in the plateau fertilized bloom area

4.4.1. Processes involved in the ML Si-isotopic balance

As discussed in Section 3.2, the plateau fertilized bloom area is defined with stations A3 and B1. In contrast to the HNLC area, estimates of the fractionation factor using the Rayleigh model (Eq. (1)) were unrealistically low ($^{30}\varepsilon$ smaller than $-0.5\permil$) compared to published $^{30}\varepsilon$ values, no matter what source and conditions were considered for the initial Si-pool (UCDW, WW on or off plateau). The ML $\delta^{30}Si_{Si(OH)_4}$ value was clearly off the Rayleigh trend (Fig. 5a), showing that Si-isotopic fractionation in the ML above the plateau could not be described with a closed system model. A high vertical nutrient supply due to high internal wave activity above the plateau is likely the reason for this situation (Park et al., 2008b). However, the ML was very close to the steady state fractionation trend when taking HNLC WW as the Si-source instead of plateau WW (Fig. 5b). This suggests that there was significant ventilation of the plateau waters by AASW from the HNLC areas located southward, in agreement with a residence time of the water above the plateau of 4 to 9 months (Venchiarutti et al., 2008; Park et al., 2008a). Since the length of the growth season in this area is about 3 months (Mongin et al., 2008), significant renewal occurs over the plateau with water advected from the south (Park et al., 2008a). Thus the whole water mass above the plateau may have been significantly ventilated with AASW from the HNLC area over the time scale of the season. This condition could explain why HNLC WW represented a relevant source with appropriate initial Si-pool conditions for the plateau ML.

Although the near complete $Si(OH)_4$ utilization in plateau surface waters should have resulted in $\delta^{30}Si_{bSiO_2}$ close to the initial $\delta^{30}Si_{Si(OH)_4}$ value, the average $\delta^{30}Si_{bSiO_2}$ in the ML was $+2.3 \pm 0.1\permil$ (Table 4). This is significantly heavier than the initial $\delta^{30}Si_{Si(OH)_4}$ values of $+1.9\permil$ (for fertilized area WW) or $+1.5\permil$ (for HNLC WW). $\delta^{30}Si_{bSiO_2}$ values exceeding $\delta^{30}Si$ of the Si-source have been reported earlier for strongly Si-depleted surface waters in the Antarctic Zone (Varela et al., 2004). Vertical mixing events can advect light Si-isotopes into the ML and therefore decreasing the difference between $Si(OH)_4$ and bSiO$_2$ $\delta^{30}Si$. However, such a process cannot explain why bSiO$_2$ isotopic composition is heavier than the source. $\delta^{30}Si_{bSiO2}$ values exceeding those of silicate in source waters can actually fit a Rayleigh model where bSiO$_2$ is exported and ML bSiO$_2$ represents the
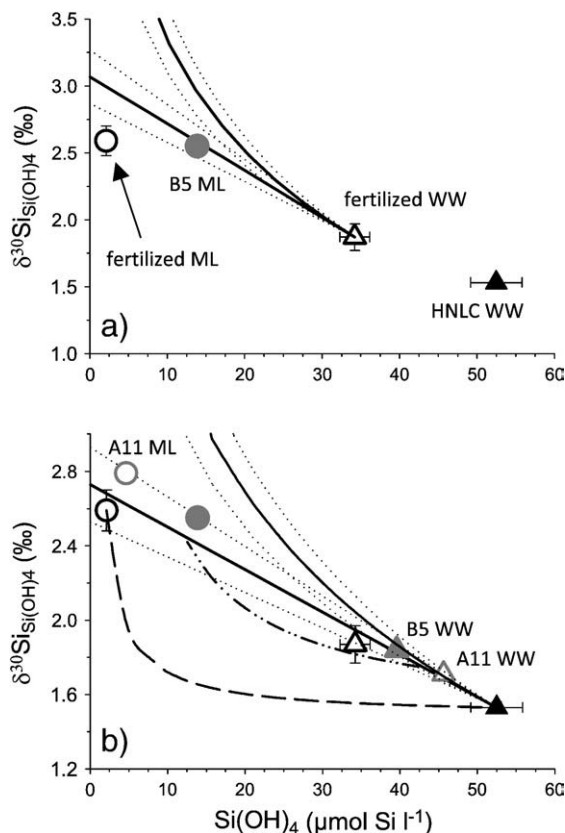
Fig. 5. $\delta^{30}Si_{Si(OH)_4}$ vs. [Si(OH)$_4$] for the different Si-pools in the fertilized (plateau) bloom area (± 1 SD; stations A3 and B1) and for HNLC WW (stations B11 and C11): (a) plateau fractionation trends following the steady state (straight line) or Rayleigh (curve) models with fertilized WW as the Si-source and the average ACC fractionation factor (-1.2 ± 0.2‰); (b) fractionation trends following the steady state (straight line) or Rayleigh (curve) model with HNLC WW as the Si-source and the average ACC fractionation factor (-1.2 ± 0.2‰). Mixing lines with HNLC WW and fertilized ML (dashed line). An example of the mixing line between hypothetical fertilized ML and a WW having undergone Si uptake (dashed–dotted line) is given. The circles and triangles represent ML and WW respectively. The black empty symbols are for the fertilized area, the empty grey for A11, the filled grey for B5, and the filled black for HNLC area. The area averages and error bars were calculated based on the mean values for each station.

instantaneous product (Eq. (2)). A mixture between accumulated and instantaneous bSiO$_2$ pools could yield a similar result. Yet, for several reasons that were discussed above a closed model cannot explain the $\delta^{30}Si_{Si(OH)_4}$ signatures that were observed in this study for the plateau area. Nevertheless, we can expect a higher uptake/mixing ratio at the bloom peak yielding a mixed layer more appropriately described by a closed system. When the mixed layer becomes Si-depleted with progression of the growth season, the uptake/mixing ratio decreases to values lower than at the beginning of the growth season. Subsequent vertical mixing supplying isotopically light Si(OH)$_4$ could then better mimic a steady state for Si(OH)$_4$ but not for bSiO$_2$. Another explanation is dissolution of biogenic silica, with preferential release of light Si-isotopes (Demarest et al., 2009). This would partly counteract the isotopic fractionation associated with biogenic silica production and decrease Δ^{30}Si, with bSiO$_2$ and Si(OH)$_4$ isotopic compositions becoming heavier and lighter, respectively (Eq. (8)). This could have been the case more particularly above the plateau because (i) significant heterotrophic activity − needed to remove frustule organic before the start of bSiO$_2$ dissolution (Bidle and Azam, 1999) was taking place (Lefèvre et al., 2008) in this senescent bloom phase (Blain et al., 2007; Mosseri et al., 2008); (ii) dead diatom cells contributed on average to as much as 15 ± 4% of total diatom cells at A3 (Armand et al., 2008); and (iii) the biogenic silica pool was larger than the Si(OH)$_4$ pool (Tables 1 and 4).

At B5 on the plateau the Δ^{30}Si value of -0.9‰ was not significantly different from the ACC $^{30}\varepsilon$ value (-1.2 ± 0.2‰). Si-depletion at B5 was not large enough to discern between the different fractionation model outputs (Fig. 5). Though a shift of the bloom toward B5 was observed at the end of KEOPS (Mongin et al., 2008), the bSiO$_2$:Si(OH)$_4$ ratio at B5 was 0.2 (compared to 1.5 ± 0.6 for A3-1, A3-2, and B1), indicating that at B5 any isotopic effect due to dissolution of biogenic silica would not be significant enough to affect the larger Si(OH)$_4$ pool. Possible vertical mixing would have little impact on Δ^{30}Si at the B5 site, since the concentration difference between the surface and subsurface was small compared to A3.

4.4.2. Processes involved in the WW Si-isotopic balance

We observed gradients in WW Si(OH)$_4$ concentrations between plateau and off-plateau stations with margin stations showing intermediate characteristics (not shown). These gradients appeared to be controlled by isopycnal mixing of HNLC WW (typically: 52.5 μmol Si l^{-1}, $\delta^{30}Si_{Si(OH)_4} = +1.5 \pm 0.0$‰; see Fig. 3c,g) with WW of altered composition present above the plateau (typically: 34.2 μmol Si l^{-1}, $\delta^{30}Si_{Si(OH)_4} = +1.9 \pm 0.1$‰; see Fig. 3c,g). Two processes could explain the alteration of the plateau WW in summer:

(1) Silicifying diatoms thriving below the plateau ML inducing a seasonal Si-depletion and $\delta^{30}Si_{Si(OH)_4}$ increase over the plateau WW. A deep bSiO$_2$ maximum was observed during the KEOPS cruise and was associated with a chlorophyll maximum (Mosseri et al., 2008; Uitz et al., 2009; Fig. 1b). The deep chlorophyll maximum is a recurrent feature in the Southern Ocean (e.g., Parslow et al., 2001; Holm-Hansen and Hewes, 2004), and several mechanisms are proposed to explain its formation (Cullen, 1982; Quéguiner et al., 1997; Parslow et al., 2001; Holm-Hansen and Hewes, 2004). For the KEOPS bloom area, Uitz et al. (2009) argue that the deep bSiO$_2$ maximum can be explained by the presence of a deep temperature driven pycnocline (well below the ML and the euphotic layer) and the sedimentation of living, though inactive, algal cells, of which the sinking rate was likely under environmental control. Brzezinski and Nelson (1989) report that diatoms can produce substantial amounts of bSiO$_2$ at depths where little or no photosynthesis is taking place. This is in agreement with numerous studies (cf. review by Martin-Jézéquel et al. (2000)) stating that energy implicated in the silicification process is mainly of respiratory origin and therefore decoupled from photosynthesis. It is thus quite possible that the deep bSiO$_2$ maximum observed in plateau WW indeed consisted of silicifying diatoms that settled out of the surface waters and accumulated at a second density gradient. Isotopic fractionation by such WW diatoms would thus placed plateau WW on a fractionation trend. Fig. 5b shows this is the case (either closed or open system fractionation trends could work) at least when HNLC WW is imposed as the original Si-source. The ML and WW at stations B5 and A11 also fell along the same fractionation trend (Fig. 5b). Si-utilization in the ML and WW at B5 was less than in the fertilized area. The observation that the bloom patch over time drifted from A3–B1 sites toward B5 (Mongin et al., 2008; Mosseri et al., 2008) supports the fact that the bloom was at a less developed stage at B5. Note that at A11 we also observed a large deep bSiO$_2$ maximum (6.3 μmol l^{-1} at 150 m; Fig. 2d), indicating that WW might have also undergone seasonal Si uptake (Fig. 5b).

(2) An alternative process that could have decreased the WW Si(OH)$_4$ concentration and increased the WW $\delta^{30}Si_{Si(OH)_4}$ is mixing between ML and WW. To test whether the observed Si concentrations and isotopic compositions could be explained by a mixing-only scenario we conducted a sensitivity analysis of the bloom area WW with the mixing line between the bloom area ML

and HNLC WW. Fig. 5b clearly shows that bloom area WW does not fit on this mixing line, but fits well on the steady state fractionation line. Mixing lines with HNLC WW and ML for B5 and A11 also could not explain their WW Si characteristics.

This result confirms that Si uptake in the subsurface is largely the dominant process controlling $Si(OH)_4$ contents and isotopic composition of WW in the fertilized bloom area and also at stations A11 and B5. An example of mixing between the ML and WW, having undergone Si uptake is also shown in Fig. 5b. While the latter scenario cannot be rejected it appears difficult to verify and would require Si uptake in the subsurface.

4.4.3. Silicon mass balance

Using HNLC WW characteristics to represent the initial conditions $(52.5 \pm 3.3\ \mu mol\ Si\ l^{-1})$ of WW in the fertilized area, we estimate the seasonal depletion in the upper 100 m at $5.0 \pm 0.3\ mol\ Si\ m^{-2}\ yr^{-1}$. For the 100 to 400 m WW layer we calculate a seasonal depletion of $5.5 \pm 1.1\ mol\ Si\ m^2\ yr^{-1}$ based on the WW $Si(OH)_4$ concentration differences between the HNLC and fertilized areas. As discussed in Section 4.3.2, the use of Si-depletion to estimate net $bSiO_2$ production in the ML probably led to an underestimation of the latter because of the continuous supply of silicic acid from deeper layers, which is particularly important above the plateau (Park et al., 2008b). However, this underestimation should be balanced by an overestimation of the net $bSiO_2$ production in the subsurface, as both estimates are biased by the same mixing process. Therefore, we were able to calculate the total net $bSiO_2$ production in the fertilized area, by summing our ML and WW estimates, at $10.5 \pm 1.4\ mol\ Si\ m^{-2}\ yr^{-1}$ (= ML seasonal depletion + WW seasonal depletion). However, a 1-D approach as used in Section 4.3.2 to calculate mass and isotopic balances could be biased for the fertilized area because of advection from the surrounding HNLC area. Compared to previous net $bSiO_2$ production estimations in the Antarctic Zone (2.4 to 3.3 mol Si $m^{-2}\ yr^{-1}$; in Pondaven et al., 2000; Nelson et al., 2002; Pollard et al., 2006), we estimate that the Kerguelen Plateau sustained an extremely high integrated net $bSiO_2$ production (see also Mosseri et al., 2008) in the higher range of the opal export estimation for the Southern Ocean (Jin et al., 2006). Natural iron fertilization, as discussed in Mosseri et al. (2008), clearly boosts diatom productivity, as observed in artificial iron fertilization (de Baar et al., 2005; Cavagna et al., in press).

5. Conclusions

The silicon cycle at two contrasting areas was studied during the KEOPS expedition (KErguelen Ocean and the Plateau compared Study) in the Antarctic Zone. We studied the HNLC area outside the Kerguelen Plateau and the natural iron-fertilized area above the plateau. The Si-isotopic data presented here allows for a better constraint of the silicon mass budget as it enabled the identification of the initial pre-bloom conditions and the different potential Si-pools involved. Seasonal Si uptake and export could then be calculated using mass and isotopic balances.

In the HNLC area, remnant WW represented the initial Si-pool of the summer ML. Si was supplied to the ML from a UCDW contribution $(4.0 \pm 0.7\ mol\ Si\ m^{-2}\ yr^{-1})$, which should be balanced by annual net $bSiO_2$ production. However, the Si-depletion over the growth season obtained from a mass balance calculation was only $2.5 \pm 0.2\ mol\ Si\ m^2\ yr^{-1}$, $1.5 \pm 0.7\ mol\ Si\ m^{-2}\ yr^{-1}$ lower than the UCDW supply. Since the seasonal Si-depletion does not take into account Si-supply during the stratification season, this difference could represent a mixing supply from below the mixed layer and suggests that the system operated more in open mode with significant Si-supply from WW.

In the natural iron-fertilized waters above the Kerguelen Plateau, the ML Si-isotopic signatures could not be reconstructed by Rayleigh

(closed system) equations. This provides firm evidence of a Si-supply to the ML during the growth season. This is in accordance with physics, which shows that the Kerguelen Plateau is a highly dynamic system. HNLC WW represents the most likely Si-source and initial pre-bloom conditions. We estimated a net $bSiO_2$ production for the bloom area AASW at $10.5 \pm 1.3\ mol\ Si\ m^{-2}\ yr^{-1}$, with a significant contribution from diatom silicification in the deep $bSiO_2$ maximum. In the fertilized area above the plateau surrounded by HNLC waters, the assumption that the system operates in 1-D mode when calculating mass and isotopic balances has to be taken with caution, since advection could be significant. Moreover, heavier $\delta^{30}Si_{bSiO_2}$ values compared to the Si-source (Winter Water) suggest that: (1) A significant part of the senescent $bSiO_2$ pool in the ML was probably already dissolved and/or (2) the system operates in a Rayleigh mode in the beginning of the Si-depletion (higher uptake/supply ratio), but significant supply (decreasing uptake/uptake ratio) at the end decreases the $\delta^{30}Si_{Si(OH)_4}$ significantly, without affecting the $\delta^{30}Si_{bSiO_2}$, when the surface $Si(OH)_4$ pool is strongly depleted. For the application of $\delta^{30}Si$ proxy in palaeoceanography, the isotopic decoupling between $bSiO_2$ and $Si(OH)_4$ has significant implications. Process studies aiming at the full characterization of the Si-processes (i.e., assessment of uptake, dissolution, export; $\delta^{30}Si$ signatures, actively bSi forming cells via PDMPO-labeling, dead/living cell ratios, …) are necessary to better constrain the origin and fate of $\delta^{30}Si_{bSiO_2}$ in the water column.

Finally, using the off-plateau KEOPS $\delta^{30}Si_{Si(OH)_4}$, where the silicon mass balance was better constrained, along with previous studies in the ACC, we refined the ACC fractionation factor estimate $(^{30}\varepsilon)$ to $-1.2 \pm 0.2‰$.

References

Abraham, K., Opfergelt, S., Fripiat, F., Cavagna, A.-J., de Jong, J.T.M., Foley, S.F., André, L., Cardinal, D., 2008. $\delta^{30}Si$ and $\delta^{29}Si$ determinations on USGS BHVO-1 and BHVO-2 reference materials with a new configuration on an Nu Plasma Multi-Collector ICP-MS. Geost. Geoanal. Res. 32 (2), 193–202.

Alleman, L., Cardinal, D., Cocquyt, C., Plisnier, P.D., Descy, J.-P., Kimirei, I., Sinyinza, D., André, L., 2005. Silicon isotopic fractionation in Lake Tanganyika and its main tributaries. J. Gt. Lakes Res. 31, 509–519.

Armand, L.K., Cornet-Barthaux, V., Mosseri, J., Quéguiner, B., 2008. Late summer diatom biomass and community structure on and around the naturally iron-fertilised Kerguelen Plateau in the Southern Ocean. Deep-Sea Res. II 55, 653–678.

Basile-Doelsh, I., 2006. Si stable isotopes in the earth's surface: a review. J. Geochem. Explor. 88, 252–256.

Beucher, C., Tréguer, P., Hapette, A.-M., Corvaisier, R., 2004. Intense summer Si-recycling in the surface Southern Ocean. Geophys. Res. Lett. 31. doi:10.1029/2003GL018998.

Beucher, C.P., Brzezinski, M.A., Jones, J.L., 2008. Sources and biological fractionation of silicon isotopes in the Eastern Equatorial Pacific. Geochim. Cosmochim. Acta 72, 3063–3073.

Bidle, K.D., Azam, F., 1999. Accelerated dissolution of diatom silica by marine bacterial assemblages. Nature 397, 508–512.

Blain, S., Quéguiner, B., Armand, L., Belviso, S., Bombled, B., Bopp, L., Bowie, A., Brunet, C., Brussaard, C., Carlotti, F., Christaki, U., Corbière, A., Durand, I., Ebersback, F., Fuda, J.L., Garcia, N., Gerringa, L., Griffiths, B., Guigue, C., Guillerm, C., Jacquet, S., Jeandel, C., Laan, P., Lefèvre, D., Lo Monaco, C., Malits, A., Mosseri, J., Obernosterer, I., Park, Y.-P., Picheral, M., Pondaven, P., Remenyi, T., Sandroni, V., Sarthou, G., Savoye, N., Scouarnec, L., Souhaut, M., Thuiller, D., Timmermans, K., Trull, T., Uitz, J., van Beek, P., Veldhuis, M., Vincent, D., Viollier, E., Vong, L., Wagener, T., 2007. Effect of natural iron fertilization on carbon sequestration in the Southern Ocean. Nature 446. doi:10.1038/nature05700, 1070–1075.

Boyd, P.W., 2007. Biogeochemistry: iron findings. Nature 446, 989–991.

Brzezinski, M.A., Nelson, D.M., 1989. Seasonal changes in the silicon cycle within a Gulf Stream warm-core ring. Deep-Sea Res. 36, 1009–1030.

Brzezinski, M.A., Nelson, D.M., Franck, V.M., Sigmon, D.E., 2001. Silicon dynamics within an intense open-ocean diatom bloom in the Pacific sector of the Southern Ocean. Deep-Sea Res. II 48, 3997–4018.

Brzezinski, M.A., Jones, J.L., Azam, F., 2003. The balance between silica production and silica dissolution in the sea: insights from Monteray Bay, California, applied to the global data set. Limnol. Oceanogr. 48 (5), 1846–1854.

Brzezinski, M.A., Jones, J.L., Demarest, M.S., 2005. Control of silica production by iron and silicic acid during the Southern Ocean iron experiment (SOFeX). Limnol. Oceanogr. 50 (3), 810–824.

Buesseler, K.O., 1998. The decoupling of production and particulate export in the surface ocean. Global Biogeochem. Cycles 12 (2), 297–310.

Buesseler, K.O., Ball, L., Andrews, J., Cochran, J.K., Hirschberg, D.J., Bacon, M.P., Fleer, A., Brzezinski, M.A., 2001. Upper ocean export of particulate organic carbon and biogenic silica in the Southern Ocean along 170°W. Deep-Sea Res. II 48, 4275–4297.

Cardinal, D., Alleman, L.Y., de Jong, J., Ziegler, K., André, L., 2003. Isotopic composition of silicon measured by multicollector plasma source mass spectrometry in dry plasma mode. J. Anal. Atom. Spectrom. 18, 213–218.

Cardinal, D., Alleman, L.Y., Dehairs, F., Savoye, N., Trull, T.W., André, L., 2005. Relevance of silicon isotopes to Si-nutrient utilization and Si-source assessment in Antarctic waters. Global Biogeochem. Cycles 19, GB2007. doi:10.1029/2004GB002364.

Cardinal, D., Savoye, N., Trull, T.W., Dehairs, F., Kopczynska, E.E., Fripiat, F., Tison, J.L., André, L., 2007. Silicon isotopes in spring Southern Ocean diatoms: large zonal changes despite homogeneity among size fractions. Mar. Chem. 106, 46–62.

Cavagna, A.-J., Fripiat, F., Dehairs, F., Wolf-Gladrow, D., Cisewski, B., Savoye, N., André, L., Cardinal, D., in press. Silicon uptake and supply during a Southern Ocean iron fertilization experiment (EIFEX) tracked by Si isotopes. Limnol. Oceanogr.

Cullen, J.J., 1982. The deep chlorophyll maximum: comparing vertical profiles of chlorophyll a. Can. J. Fish. Aquat. Sci. 39 (5), 791–803.

De Baar, H.J.W., Boyd, P.W., Coale, K.H., Landry, M.R., Tsuda, A., Assmy, P., Bakker, D.C.E., Bozec, Y., Barber, R.T., Brzezinski, M.A., Buesseler, K.O., Boyé, M., Croot, P.L., Gervais, F., Gorbunov, M.Y., Harrison, P.J., Hiscock, W.T., Laan, P., Lancelot, C., Law, C.S., Levasseur, M., Marchetti, A., Millero, F.J., Nishioka, J., Nojiri, H., Takeda, S., Timmermans, K.R., Veldhuis, M.J.W., Waite, A.M., Wong, C.S., 2005. Synthesis of iron fertilization experiments: from the iron age in age of enlightenment. J. Geophys. Res. 110, C09S16. doi:10.1029/2004JC002601.

De La Rocha, C.L., Brzezinski, M.A., DeNiro, M.J., 1996. Purification recovery and laser-driven fluorination of silicon from dissolved and particulate silica for the measurement of natural stable isotope abundances. Anal. Chem. 68, 3746–3750.

De la Rocha, C.L., Brzezinski, M.A., DeNiro, M.J., 1997. Fractionation of silicon isotopes by marine diatoms during biogenic silica formation. Geochim. Cosmochim. Acta 61 (23), 5051–5056.

De la Rocha, C.L., Brzezinski, M.A., DeNiro, M.J., 2000. A first look at the distribution of the stable isotopes of silicon in natural waters. Geochim. Cosmochim. Acta 64 (14), 2467–2477.

Demarest, M.S., Brzezinski, M.A., Beucher, C.P., 2009. Fractionation of silicon isotopes during biogenic silica dissolution. Geochim. Cosmochim. Acta 73 (19), 5572–5583.

Douthitt, C.B., 1982. The geochemistry of the stable isotopes of silicon. Geochim. Cosmochim. Acta 46, 1449–1458.

Dugdale, R.C., Wilkerson, F.P., Minas, H.J., 1995. The role of a silicate pump in driving new production. Deep-Sea Res. I 42 (5), 697–719.

François, R., Altabet, M.A., Goericke, R., McCorkle, D.C., Brunet, C., Poisson, A., 1993. Changes in the δ13C of surface water particulate organic matter across the subtropical convergence in the SW Indian Ocean. Global Biogeochem. Cycles 7 (3), 627–644.

Fripiat, F., Cardinal, D., Tison, J.-L., Worby, A., André, L., 2007. Diatom-induced silicon isotopic fractionation in Antarctic sea ice. J. Geophys. Res. 112, G02001. doi:10.1029/2006JG000244.

Georg, R.B., Halliday, A.N., Schauble, E.A., Reynolds, B.C., 2007. Silicon in the Earth's core. Nature 447, 1102–1106.

Grasshoff, K., Erhardt, M., Kremling, K., 1983. Methods of seawater analysis, 2nd ed. Verlag Chemie, Weinheim.

Hildebrand, M., 2008. Diatoms, biomineralization processes, and genomics. Chem. Rev. 108, 4855–4874.

Holm-Hansen, O., Hewes, C.D., 2004. Deep chlorophyll-a maxima (DCMs) in Antarctic waters: I. Relationships between DCMs and the physical, chemical, and optical conditions in the upper water column. Polar. Biol. 27, 699–710.

Jeandel C., Peucker-Ehrenbrink, Y. Godderis, F. Lacan, O. Aumont and T. Arsouze. Ocean margin processes affect biogeochemical cycles of climate-relevant elements Si, Ca, Mg and Fe. Submitted to Nature Geoscience.

Jin, X., Gruber, N., Dunne, J.P., Sarmiento, J.L., Amstrong, R.A., 2006. Diagnosing the contribution of phytoplankton functional groups to the production and export of particulate organic carbon, CaCO3, and opal from global nutrient and alkalinity distributions. Global Biogeochem. Cycles 20, GB2015. doi:10.1029/2005GB002532.

Karl, D.M., Tien, G., 1992. MAGIC: a sensitive and precise method for measuring dissolved phosphorus in aquatic environments. Limnol. Oceanogr. 37, 105–116.

Lefèvre, D., Guigue, C., Obernosterer, I., 2008. The metabolic balance at two contrasting sites in the Southern Ocean: the iron-fertilized Kerguelen area and HNLC waters. Deep-Sea Res. II 55, 766–776.

Martin-Jézéquel, V., Hildebrand, M., Brzezinski, M.A., 2000. Silicon metabolism in diatoms: implications for growth. J. Phycol. 36, 821–840.

Milligan, A.J., Varela, D.E., Brzezinski, M.A., Morel, F.M.M., 2004. Dymanics of silicon metabolism and silicon isotopic discrimination in a marine diatom as a function of pCO2. Limnol. Oceanogr. 49 (2), 322–329.

Mongin, M., Molina, E., Trull, T.W., 2008. Seasonality and scale of the Kerguelen Plateau phytoplankton bloom: a remote sensing and modeling analysis of the influence of natural iron fertilization in the Southern Ocean. Deep-Sea Res. II 55, 880–892.

Mosseri, J., Quéguiner, B., Armand, L., Cornet-Barthaux, V., 2008. Impact of iron on silicon utilization by diatoms in the Southern Ocean: a case study of Si/N cycle decoupling in a naturally iron enriched area. Deep-Sea Res. II 55, 801–819.

Nelson, D.M., Brzezinski, M.A., Sigmon, D.E., Franck, V.M., 2001. A seasonal progression of Si limitation in the Pacific sector of the Southern Ocean. Deep-Sea Res. II 48, 3973–3995.

Nelson, D.M., Anderson, R.F., Barber, R.T., Brzezinski, M.A., Buesseler, K.O., Chase, Z., Collier, R.W., Dickson, M.L., François, R., Hiscock, M.R., Honjo, S., Marra, J., Martin, W.R., Sambrotto, R.J., Sayles, F.L., Sigmon, D.E., 2002. Vertical budgets for organic carbon and biogenic silica in the Pacific sector of the Southern Ocean, 1996–1998. Deep-Sea Res. II 49, 1645–1674.

Park, Y.-H., Charriaud, E., Ruiz Pino, D., Jeandel, C., 1998a. Seasonal and interannual variability of the mixed layer properties and steric height at station KERFIX, southwest of Kerguelen. J. Mar. Sys. 17, 571–586.

Park, Y.-H., Charriaud, E., Fieux, M., 1998b. Thermohaline structure of the Antarctic Surface Water/Winter Water in the Indian sector of the Southern Ocean. J. Mar. Sys. 17, 5–23.

Park, Y.-H., Roquet, F., Durand, I., Fuda, J.L., 2008a. Large-scale circulation over and around the Northern Kerguelen Plateau. Deep-Sea Res. II 55, 566–581.

Park, Y.-H., Fuda, J.L., Durand, I., Naveira Garabato, A.C., 2008b. Internal tides and vertical mixing overt the Kerguelen Plateau. Deep-Sea Res. II 55, 582–593.

Parslow, J.S., Boyd, P.W., Rintoul, S.R., Griffiths, F.B., 2001. A persistent subsurface chlorophyll maximum in the Interpolar Frontal Zone south of Australia: seasonal progression and implications for phytoplankton–light–nutrient interactions. J. Geophys. Res. 106 (C12), 31543–31557.

Pollard, R.T., Tréguer, P., Read, J., 2006. Quantifying nutrient supply to the Southern Ocean. J. Geophys. Res. 111, C05011. doi:10.1029/2005JC003076.

Pondaven, P., Ragueneau, O., Tréguer, P., Hauvespre, A., Dezileau, L., Reyss, J.L., 2000. Resolving the «opal paradox» in the Southern Ocean. Nature 405, 168–172.

Quéguiner, B., Brzezinski, M.A., 2002. Biogenic silica production rates and particulate matter distribution in the Atlantic sector of the Southern Ocean during austral spring. Deep-Sea Res. II 49, 1765–1786.

Quéguiner, B., Tréguer, P., Peeken, I., Scharek, R., 1997. Biogeochemical dynamics and the silicon cycle in the Atlantic sector of the Southern Ocean during austral spring. Deep-Sea Res. II 44, 69–89.

Ragueneau, O., Savoye, N., Del Amo, Y., Cotten, J., Tardiveau, B., Leynaert, A., 2005. A new method for the measurement of biogenic silica in suspended matter of coastal waters: using Si:Al ratio to correct for the mineral interference. Cont. Shelf Res. 25, 697–710.

Reynolds, B.C., Frank, M., Halliday, A.N., 2006. Silicon isotope fractionation during nutrient utilization in the North Pacific. Earth Planet. Sci. Lett. 244, 431–443.

Reynolds, B.C., Aggarwal, J., André, L., Baxter, D., Beucher, C., Brzezinski, M.A., Engström, E., Georg, R.B., Land, M., Leng, M.J., Opfergelt, S., Rodushkin, I., Sloane, H.J., van den Boorn, H.J.M., Vroon, P.Z., Cardinal, D., 2007. An inter-laboratory comparison of Si isotope reference materials. J. Anal. Atom. Spectrom. 22, 561–568.

Sarmiento, J.L., Gruber, N., Brzezinski, M.A., Dunne, J.P., 2004. High-latitude controls of thermocline nutrients and low latitude biological productivity. Nature 427, 56–60.

Sarmiento, J.L., Simeon, J., Gnanadesikan, A., Gruber, N., Key, R.M., Schlitzer, R., 2007. Deep ocean biogeochemistry of silicic acid and nitrate. Global Biogeochem. Cycles 21, GB1S90. doi:10.1029/2006GB002720.

Savoye, N., Trull, T.W., Jacquet, S.H.M., Navez, J., Dehairs, F., 2008. 234Th-based export fluxes during a natural iron fertilization experiment in the Southern Ocean (KEOPS). Deep-Sea Res. II 55, 841–855.

Sigman, D.M., Altabet, M.A., McCorkle, D.C., François, R., Fischer, G., 1999. The δ15N of nitrate in the Southern Ocean: consumption of nitrate in surface waters. Global Biogeochem. Cycles 13, 1149–1166.

Sigman, D.M., Karsh, K.L., Casciotti, K.L., 2009. Nitrogen isotopes in the ocean. In: Steele, J.H., Turekian, K.K., Thorpe, S.A. (Eds.), Encyclopedia of Ocean Sciences (update from 2001). Academic Press, London.

Sokolov, S., Rintoul, S.R., 2007. On the relationship between fronts of the Antarctic Circumpolar Current and surface chlorophyll concentration in the Southern Ocean. J. Geophys. Res. 112, C07030. doi:10.1029/2006JC004072.

Taylor, S.R., McLennan, S.M., 1985. The continental crust: its composition and evolution. Blackwell Scientific Publications, Oxford, p. 312.

Tréguer, P., Jacques, G., 1992. Dynamics of nutrients and phytoplankton, and fluxes of carbon, nitrogen and silicon in the Antarctic Ocean. Polar Biol. 12, 149–162.

Tréguer, P., Nelson, D.M., van Bennekom, A.J., DeMaster, D.J., Leynaert, A., Quéguiner, B., 1995. The silica balance in the world ocean: a re-estimate. Science 268, 375–379.

Uitz, J., Claustre, H., Griffiths, F.B., Ras, J., Garcia, N., Sandroni, V., 2009. A phytoplankton class-specific primary production model applied to the Kerguelen Islands region (Southern Ocean). Deep-Sea Res. I 56, 541–560.

Varela, D.E., Pride, C.J., Brzezinski, M.A., 2004. Biological fractionation of silicon isotopes in Southern Ocean surface waters. Global Biogeochem. Cycles 18, GB1047. doi:10.1029/2003GB002140.

Venchiarutti, C., Jeandel, C., Roy-Barman, M., 2008. Particle dynamics study in the wake of Kerguelen Island using thorium isotopes. Deep-Sea Res. I 55, 1343–1363.

Young, E.D., Galy, A., Nagahara, H., 2002. Kinetic and equilibrium mass-dependent isotope fractionation laws in nature and their geochemical and cosmochemical significance. Geochim. Cosmochim. Acta 66 (6), 1095–1104.

Zhang, Y., Lacan, F., Jeandel, C., 2008. Dissolved rare earth elements tracing lithogenic inputs over the Kerguelen Plateau (Southern Ocean). Deep-Sea Res. II 55, 638–652.

Ziegler, K., Chadwick, O.A., Brzezinski, M.A., Kelly, E.F., 2005. Natural variations of δ30Si ratios during progressive basalt weathering, Hawaiian Islands. Geochim. Cosmochim. Acta 69 (19), 4597–4610.